ACS OMEGA

Article

Cite This: ACS Omega 2019, 4, 15240−15248

http://pubs.acs.org/journal/acsodf

Theranostic Lysosomal Targeting Anticancer and Antimetastatic Agents: Half-Sandwich Iridium(III) Rhodamine Complexes

Wenli Ma,[†] Xingxing Ge,[†] Zhishan Xu,[†,‡] Shumiao Zhang,[†] Xiangdong He,[†] JuanJuan Li,[†] Xiaorong Xia,[†] Xiaobing Chen,[†] and Zhe Liu*[,†]

[†]Institute of Anticancer Agents Development and Theranostic Application, The Key Laboratory of Life-Organic Analysis and Key Laboratory of Pharmaceutical Intermediates and Analysis of Natural Medicine, Department of Chemistry and Chemical Engineering, Qufu Normal University, Qufu 273165, China

[‡]Department of Chemistry and Chemical Engineering, Shandong Normal University, Jinan 250014, China

Supporting Information

ABSTRACT: Two rhodamine-modified half-sandwich Ir(III) complexes with the general formula $[(Cp^x)Ir(\hat{C}N)\ Cl]$ were synthesized and characterized, where Cp^x is 1-biphenyl-2,3,4,5-tetramethylcyclopentadienyl (Cp^{xbiph}). Both complexes showed potent anticancer activity against A549, HeLa, and HepG2 cancer cells and normal cells, and altered ligands had an effect on proliferation resistance. The complex enters cells through energy dependence, and because of the different ligands, not only could it affect the anticancer ability of the complex but also could affect the degree of complex lysosome targeting, lysosomal damage, and further prove the antiproliferative mechanism of the complex. Excitingly, antimetastatic experiments demonstrated that complex **1** has the ability to block the migration of cancer cells. Furthermore, although the complex did not show a stronger ability to interfere with the coenzyme NAD^+/NADH pair by transfer hydrogenation, the intracellular reactive oxygen species (ROS) content has shown a marked increase. NF-κB activity is increased by ROS regulation, and the role of ROS-NF-κB signaling pathway further induces apoptosis. Moreover, cell flow experiments also demonstrated that complex **1** blocked the cell cycle in S phase, but the complex did not cause significant changes in the mitochondrial membrane potential.

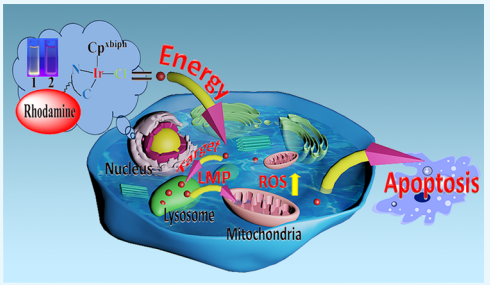

1. INTRODUCTION

Cancer has become one of the main fatal diseases worldwide, which has surpassed cardiovascular diseases as the leading cause of death.[1−3] Therefore, research on anticancer drugs cannot be delayed. Metal-based anticancer drug therapy is a valuable class of drugs in oncology research, including imaging applications, examples of novel chemotherapeutic agents, and important research values in diagnostics and clinical trials.[4] A platinum-based drug is one of the most commonly used drugs for the treatment of various human cancers, but they still have shortcomings such as poor drug resistance and serious side effects and so on.[5] For these reasons, more and more researchers are turning their attention to other alternative transition-metal complexes. As new iridium complexes have been reported to have selective biological activity and to overcome the resistance of platinum-based therapies, the development of antitumor iridium complexes therapeutics has been of great interest to researchers.[6−19]

On the other hand, it has been reported that the fluorescent ring metallated Ir(III) complex exerts powerful anticancer effects through different mechanisms, such as targeting subcellular organelles and inhibiting proteins activities.[20,21] However, there is not much research on the anticancer mechanism of half-sandwich iridium complexes without fluorescence.[22,23] The study of lysosomal targeted half-sandwich complexes has attracted a lot of interest from researchers. It is well known that lysosomes are important acidic cell organelles for decomposing biological macromolecules such as proteins, nucleic acids, and polysaccharides; when the cell ages, its lysosome ruptures, releasing hydrolase, digesting the entire cell, and causing it to die.[24,25] In cancer cells, the lysosomes will be larger, more unstable, more numerous, and exhibit more hydrolytic enzymes (such as cathepsins) than normal cells.[26,27] Additionally, when lysosomal targeted drugs enter cells, they accumulate specifically in lysosomes, leading to changes in the osmotic pressure in lysosomes and in turn causing lysosomal swelling, rupture, and lysosomal membrane permeabilization (LMP).[26,28] The escape of a hydrolase leads to autolysis of the cell, which in turn induces cell death.[29−31]

It is well known that derivatives of rhodamine usually have excellent fluorescent properties.[32,33]

Inspired by the pioneering work of Czarnik and colleagues, rhodamine derivatives are often used as fluorescent chemicals.[34,35] Thus, various rhodamine-based fluorescent probe metal cations have been reported over the past few years.[36−38]

Received: July 15, 2019
Accepted: July 30, 2019
Published: September 3, 2019

DOI: 10.1021/acsomega.9b01863
ACS Omega 2019, 4, 15240−15248

Scheme 1. Structure of Relevant Iridium(III) Complexes and Our Current Work

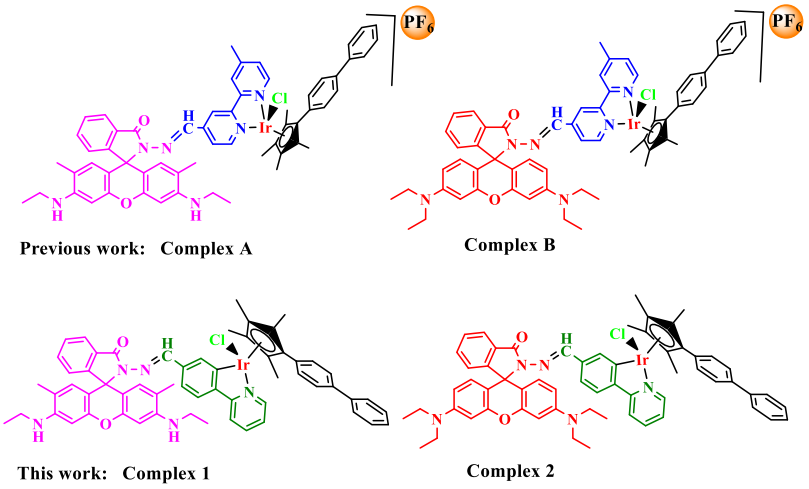

Scheme 2. Synthesis of L_1–L_2 and Complexes 1–2

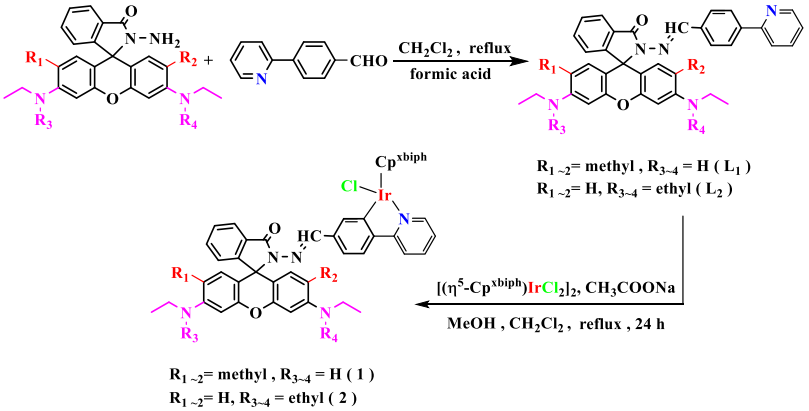

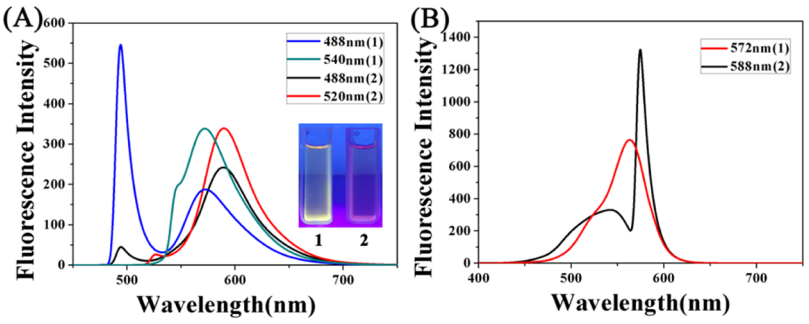

Figure 1. (A) Emission spectra of complexes **1**–**2** (10 μM) measured in CH_3CN at 298 K (excitation at 488 nm and 520/540 nm). (B) Excitation spectra of complexes **1**–**2** (10 μM) measured in CH_3CN at 298 K (emission at 588/572 nm).

Besides, rhodamine-modified complexes generally have excellent anticancer activity.[39−41] In addition, the ĈN-chelating ligands lead to an increase in the hydrophobicity of the complexes, resulting in better accumulation of the complexes in the cells,[42,43] which is more conducive to studying the anticancer mechanism of fluorescent complexes. Besides, we have studied the rhodamine-modified N̂N-chelating ligands for half-sandwich iridium(III) complexes before, with the increase of the phenyl group in the tetramethylcyclopentadienyl ring, the complexes would show better anticancer ability.[12,39,41,44] Herein, we designed and synthesized a new type of half-sandwich iridium complex (Scheme 1). It is well known that both rhodamine B and rhodamine 6G are good dyes. By introducing these two fluorophores, a new ĈN ligand is constructed to make the complexes exhibit fluorescent characteristics, and the difference in antiproliferative ability and localization in the cell of the two complexes are compared, which facilitates the study of the specific anticancer mechanism of the complex in the cell. Our results showed that these newly synthesized iridium complexes have good two-photon performance, strong color development, and high targeting and have potential application values in the synthesis of cancer-targeting drugs, probe designs, and fluorescent biomarkers.

DOI: 10.1021/acsomega.9b01863
ACS Omega 2019, 4, 15240−15248

Table 1. IC_{50} Values of Complexes 1−2, Complexes A−B, and Cisplatin toward A549, HeLa, and HepG2 Cancer Cells and Normal Cells

	IC_{50} (μM)			
complex	A549	HeLa	HepG2	BEAS-2B
$[(\eta^5\text{-}C_5Me_4C_6H_4C_6H_5)Ir(L_1)Cl]PF_6$ (**1**)	23.2 ± 3.6	18.7 ± 2.7	19.4 ± 7.5	19.96 ± 0.7
$[(\eta^5\text{-}C_5Me_4C_6H_4C_6H_5)Ir(L_2)Cl]PF_6$ (**2**)	36.8 ± 1.6	28.2 ± 3.8	28.7 ± 6.9	30.12 ± 0.3
dimer ($[(\eta^5\text{-}Cp^{xbiph})IrCl_2]_2$)	>50	>50	>50	>50
complex A	2.6 ± 0.3	3.6 ± 0.8	5.5 ± 0.7	3.0 ± 0.2
complex B	4.3 ± 0.2	4.2 ± 0.2	5.1 ± 0.1	7.2 ± 0.6
cisplatin	21.3 ± 1.7	7.5 ± 0.2	22.7 ± 1.1	42.0 ± 2.3

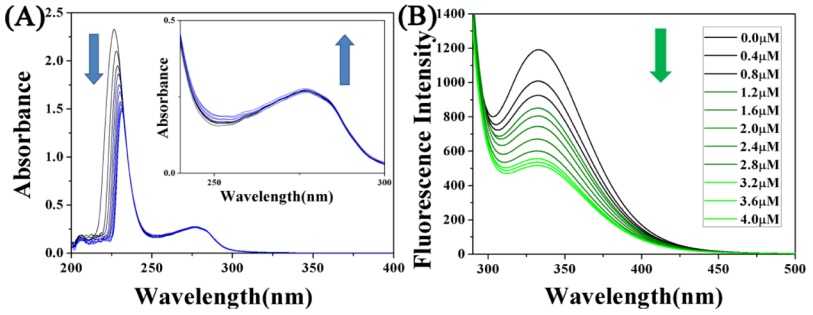

Figure 2. (A) UV−vis spectra of BSA (10 μM, 50 mM Tris-HCl, 50 mM NaCl, pH = 7.2) and complex **1** (0−4.0 μM) reaction. Arrows indicate the direction of change in absorbance. Inset: UV absorption spectra from 240 to 300 nm. (B) Fluorescence spectra of BSA (10 μM, 50 mM Tris-HCl, 50 mM NaCl, pH = 7.2) reacted with complex **1** (0−4.0 μM) (BSA: 10 μM; λ_{ex} = 280 nm; λ_{em} = 343 nm).

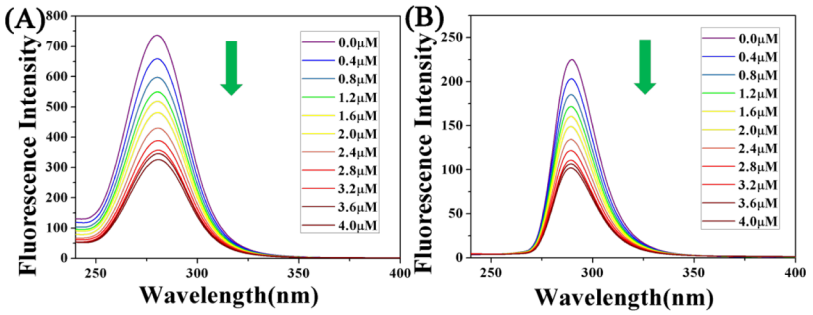

Figure 3. (A) Synchronous fluorescence spectrum of the reaction of BSA (10 μM, 50 mM Tris-HCl, 50 mM NaCl, pH = 7.2) with complex **1** (0−4.0 μM) when $\Delta\lambda$ = 60 nm, and (B) synchronous fluorescence spectrum of the reaction of BSA (10 μM, 50 mM Tris-HCl, 50 mM NaCl, pH = 7.2) with complex **1** (0−4.0 μM) at $\Delta\lambda$ = 15 nm. Arrows indicate the changes in wavelength as the compound increases.

2. RESULTS AND DISCUSSION

2.1. Synthesis, Stability, and Fluorescence Characteristics of Complexes. In this paper, a total of two new ĈN coordination iridium complexes have been synthesized. Detailed synthesis routes for ligands and complexes are shown in Scheme 2. Ligands L_1−L_2 were synthesized by the condensation of rhodamine B hydrazide (or rhodamine 6G hydrazide) with 1 equiv of 4-(2-pyridyl)-benzaldehyde in dichloromethane at a reflux temperature. These iridium complexes **1**−**2** were synthesized from the corresponding ligands in high yield (60−75%) by stirring at heating temperature with $[(\eta^5\text{-}Cp^{xbiph})IrCl_2]_2$ (dimer). The two complexes in this article were characterized by mass spectrometry and NMR spectroscopy (Figures S10−S14), and we also studied the stability and fluorescence properties of the complexes, indicating that the complex has good stability. In addition, because of the different ligands, it also has an effect on the emission of the complex. The rhodamine B-modified half-sandwich iridium complex has a larger Stokes shift (Figures 1 and S1).

2.2. Antiproliferative Studies. We evaluated the in vitro antiproliferative activity of complexes **1**−**2** using the MTT method of A549, HeLa, and HepG2 cancer cells and normal cells.[45] The IC_{50} values (half maximal inhibitory concentration) of the complexes **1**−**2** were tested (Table 1). The IC_{50} value of complex **2** is greater than complex **1** because of the difference in the ligand. This is similar to the anticancer activity of complexes A and B we reported, indicating that the introduction of rhodamine 6G can increase the anticancer activity of the complex. It has been previously reported that the complex of ĈN ligand has better anticancer activity than N̂N,[42,46] but interestingly, the activity of complexes **1** and **2**, which is designed to synthesize a ĈN ligand, is not as good as complexes A and B.[39,41] The reason for this result may be due to the enhanced lipophilicity of the neutral complex containing the ĈN ligand, while the cationic complex with the N̂N ligand is more hydrophobic, resulting that the anticancer activity of complexes **1** and **2** is rather lowered. In addition, we have compared the anticancer activity of complexes **1** and **2** and dimer; the experimental results show that by introducing a fluorophore, the anticancer activity of the complex can be

DOI: 10.1021/acsomega.9b01863
ACS Omega 2019, 4, 15240−15248

increased. Therefore, the ligand could not only affect the fluorescence characteristics of the complexes but also affect the antiproliferation ability of the complexes.

2.3. BSA Binding Studies. Serum albumin is abundant in plasma and has significant binding properties, playing a vital role in drug delivery systems. The reaction of metal-based anticancer agents with proteins may have significance in cytotoxicity, biodistribution, and even the mechanism of action of anticancer agents and thus has attracted widespread attention.[47,48] In order to study the transport of complexes into the human body.[49−51] The interaction between complex **1** and bovine serum albumin (BSA) is taken as an example (Figure 2).[52,53] The specific experimental steps are supplemented in the Supporting Information The experimental results show that complexes **1** and **2** have stronger degree of binding to BSA than previously reported complex A (K_b = 4.00 × 10^4 M^{-1}).

Moreover, the study of BSA by synchronous fluorescence spectroscopy studied the molecular environment near the fluorophore.[54] The characteristic information of the tyrosine residue of BSA is $\Delta\lambda$ = 15 nm in the wavelength interval and the characteristic information of tryptophan residues is in the wavelength interval $\Delta\lambda$ = 60 nm. The fluorescence spectrum is shown in Figure 3. The specific experimental steps are supplemented in the Supporting Information, and we also studied the interaction of complex **2** with BSA (Figures S2−S4). By studying the interaction between the complex and BSA, it was shown that the synthesized drug can be carried to the needed place by binding to BSA (Table 2).

Table 2. Values of K_b, K_{SV}, and K_q for Complexes 1 and 2 at 298 K

complex	T (K)	K_{SV} (10^5 M^{-1})	K_q (10^{13} M^{-1} s^{-1})	K_b (M^{-1})	n
1	298	3.42 ± 0.4	3.42	3.71 × 10^5	0.885
2	298	3.22 ± 0.2	3.22	3.31 × 10^5	0.944

2.4. Cell Cycle Arrest. To investigate the anticancer mechanism of complex entry into cells, analysis of whether complex **1** with good antiproliferative capacity can disrupt or prevent cell cycle to affect apoptosis by using flow cytometry.[55] A549 cells were treated with complex **1** at the IC_{50} concentrations of 0.25, 0.5, 1.0, and 2.0 for 24 h (Figure 4, Table S1). By flow cytometry analysis, the cells in the S phase increased by 8.58% compared to the control treatment at a complex's concentration of 2 × IC_{50}. This has similar properties to complex A with the same fluorophore. For complex A, the cells in the S phase increased by 5.90% compared to the control treatment at a complex's concentration of 2 × IC_{50}. Complex **1** is able to arrest the S phase of the cell cycle more than complex A.

2.5. Apoptosis Assay. Apoptosis plays an important role in the evolution of organisms, the development of multiple systems, and the stability of internal environment. Many metal anticancer complexes can inhibit cell growth through the apoptotic pathway.[43] We tried to use the annexin V/PI method to study whether complex **1** causes apoptosis. Annexin V was used as one of the sensitive indicators to detect early apoptosis of cells. Propidium iodide (PI) is a nucleic acid dye that does not penetrate intact cell membranes because of the increase in cell membrane permeability, metaphase, and late apoptotic cells. Therefore, annexin V/PI are used to distinguish cells at different stages of apoptosis. Flow cytometry was used to analyze the apoptosis of the complex. A549 cells were treated with 0.5, 1.0, 2.0, and 3.0 equiv of IC_{50} complex **1** for 24 h. In the A549 control experiment, only 6.34% cells (late apoptosis of early apoptosis) have undergone apoptosis. When the concentration of the complex was 3 × IC_{50}, a total of 96.71% cells (early apoptosis, late apoptosis) developed apoptosis (Figure 5, Table S2). The experimental results show that complex **1** could induce cell apoptosis and increase in a dose-dependent manner.

2.6. Cellular Localization Assay. First, using the luminescent properties of the complex, we used confocal microscopy to study the way these complexes enter the cell.[37] We selected complex **1** to study how the complexes entered the cells, pretreating A549 cells at 37 or 4 °C. Furthermore, pretreatment of A549 cells with carbonylcyanide *m*-chlorophenylhydrazone (CCCP, metabolic inhibitor 50 μM) and chloroquine (endocytosis modulator 50 μM) and laser confocal contrast experiments were performed on the samples under the same parameters. The experimental results show that at room temperature (37 °C), complex **1** (1 × IC_{50}) mainly enter the cell cytoplasm, but A549 cells treated at 4 °C and CCCP did not enter the complex (Figure 6). As a result, the efficiency of cell entry was significantly reduced, but treatment of A549 cells with chloroquine was almost the same as at room temperature. This shows that the iridium complexes in this system mainly enter into the cells in an energy-dependent manner.

Next, because of the difference in fluorophores in the ligands, the colocalization of complexes **1** and **2** (1 × IC_{50}) and Lyso Tracker Deep Red (LTDR, 500 nM) in A549 cells was different, and the homologous localization coefficients between Pearson correlation coefficients (PCC) were 0.64 and 0.87, respectively (Figure 7).[16,56] Laser confocal experiments show

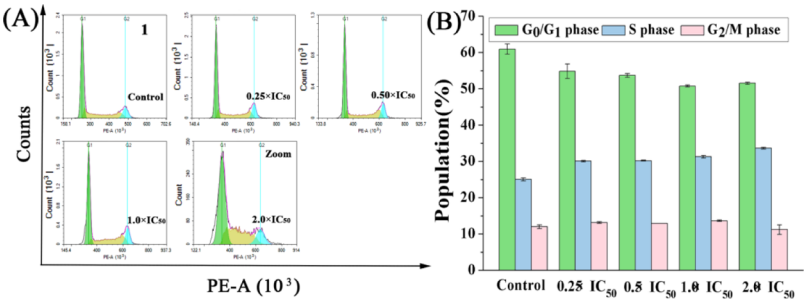

Figure 4. (A) Cell cycle analysis of A549 cancer cells after 24 h of exposure to complex **1** at 310 K. Cell staining for flow cytometry was carried out using PI/RNase. (B) A histogram of the cell cycle distribution. The data are quoted as mean ± SD of two replicates of experimental data.

DOI: 10.1021/acsomega.9b01863
ACS Omega 2019, 4, 15240−15248

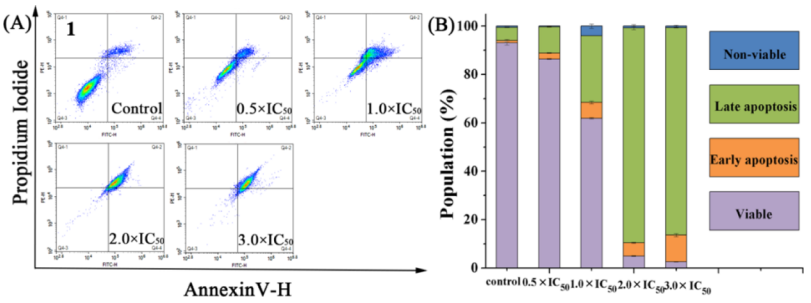

Figure 5. (A) Apoptosis analysis of A549 cancer cells after 24 h of exposure to complex **1** at 310 K determined by flow cytometry with annexin V-FITC vs PI staining. (B) Histogram showing populations for A549 cells in four stages treated by complex **1**. Data are quoted as mean ± SD of three replicates.

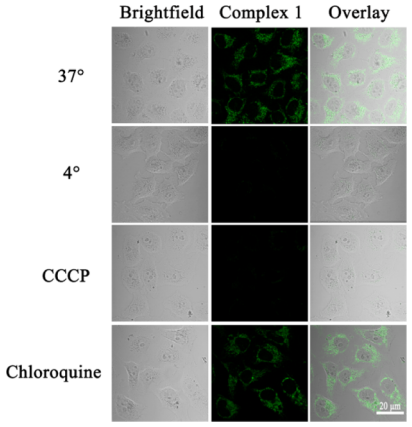

Figure 6. Effect of incubation temperature, metabolic inhibitor (CCCP, 50 μM), and chloroquine (50 μM) of complex **1** (1 × IC_{50}, 1 h) measured by a two-photon laser scanning microscope (complex: λ_{ex} = 488 nm and λ_{em} = 500−600 nm; scale bar: 20 μm).

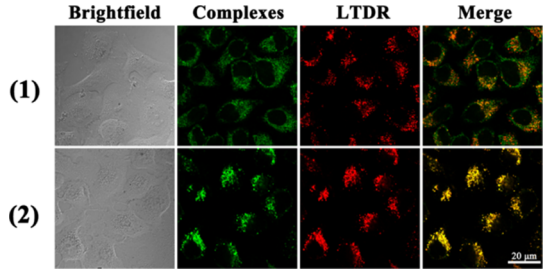

Figure 7. Intercellular colocalization of complexes **1** and **2** with LTDR. A549 cells were incubated with 1 × IC_{50} of complexes **1** and **2** and at 1 h, then stained with LTDR (500 nM, 1 h) at 310 K (complexes **1** and **2**: λ_{ex} = 488 nm and λ_{em} = 500−600 nm; LTDR, λ_{ex} = 594 nm and λ_{em} = 600−660 nm). Scale bar: 20 μm.

that complex **2** modified with rhodamine B better targets lysosome than complex **1**, and complex **1** has a stronger targeting than complex A (PCC = 0.53) with the same fluorophore. The colocalization coefficients of rhodamine B hydrazide and rhodamine 6G hydrazide and lysosome were 0.62 and 0.58, respectively.[41] This indicates that the metal-containing drug will concentrate better in lysosomes. In addition, complex and Mito Tracker Deep Red (500 nM) have not been colocated, and PCC can be ignored (Figure S5). The results indicate that the complex is distributed in the cytoplasm and can specifically target lysosomes rather than other organelles.

2.7. Lysosomal Membrane Permeabilization.

The lysosomal damage of complex **1** using the fluorescent dye acridine orange (AO) was also investigated. The fluorescent dye AO is a metachromatic dye. The single-stranded nucleic acid is an orange-red fluorescent, and the double-stranded nucleic acid is a green fluorescent. AO is weakly alkaline, and the pH inside the lysosome is low. AO can enter the lysosome through the cell membrane structure and combine with its internal hydrolase to produce orange-red fluorescence.[16,57] Studies have shown that apoptosis is accompanied by acidification of the entire cell, including the nucleus. The lysosomes may play an important role in the induction of apoptosis. When the lysosome remains substantially intact, the AO dye can accumulate in the lysosome, so more orange-red fluorescent fragments are visible in the cells. The necrotic cells that have undergone apoptosis will destroy the complete structure of the lysosome and destroy the accumulation ability of AO, so the orange-red fluorescence will be less. After treatment of A549 cells with complex **1** at 1 × IC_{50} and 2 × IC_{50}, the red fluorescence significantly decreased with increasing drug toxicity (Figure 8). Furthermore, complex **1** can cause permeabilization of the lysosomal membrane. We designed the synthesis of synthetic iridium complexes in lysosomes, which would lead to changes in the osmotic pressure of lysosomes and would cause lysosomes to swell and rupture, leading to LMP. In addition, disruption of lysosomal

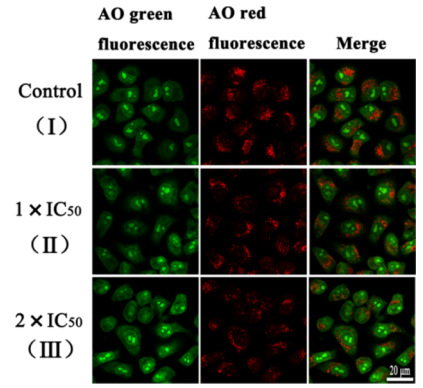

Figure 8. LMP in A549 cancer cells. (I) A549 cells without added complex **1**. A549 cells were incubated with complex **1** of 1 × IC_{50} (II) and 2 × IC_{50} (III) for 6 h and then stained with AO (5 μM, 15 min) at 310 K. The cells were measured using a two-photon laser scanning microscope (AO green fluorescence, λ_{ex} = 488 nm and λ_{em} = 510 ± 20 nm; AO red fluorescence, λ_{ex} = 488 nm and λ_{em} = 625 ± 20 nm). Scale bar: 20 μm.

DOI: 10.1021/acsomega.9b01863
ACS Omega 2019, 4, 15240−15248

membrane integrity results in the release of proteases from lysosomes into the cytosol, such as cathepsin B, which induces cell death through a variety of mechanisms.[7]

2.8. Analysis of Mitochondrial Membrane Potential. Loss of mitochondrial membrane potential (MMP) may be one of the important causes of apoptosis.[10] Fluorescence probe JC-1(5,5′,6,6′-tetrachloro-1,1′,3,3′-tetraethyl-imidacarbocyanine) is used for detecting MMP in cells by flow cytometry.[58] As the incubation concentration increased to 2 × IC_{50} of complex **1**, the percentage of cells with green fluorescence increased from 1.32 to 3.86% (Figure S6 and Table S3), indicating that complex **1** had no significant effect on MMP. It may be that the complex does not directly act on the mitochondria, so the damage to the mitochondria is low.

2.9. Induction of Reactive Oxygen Species in A549 Cancer Cells. The normal metabolism in the body can produce reactive oxygen species (ROS), but under the pathological conditions, excessive ROS usually cause damage to cells. According to reports, transition-metal-based anticancer drugs can often induce cell death by inducing cell damage.[59] Using flow cytometry, we studied changes in intracellular ROS content at various concentrations of complex **1**. The results showed that when A549 cancer cells were exposed to complex **1** for 24 h, it was observed that the level of ROS induced by complex **1** in cancer cells increased significantly in a dose-dependent manner. When the concentration of complex was 0.5 × IC_{50}, the content of ROS was increased by 2.5 times compared with the control group (Figure 9). This indicates

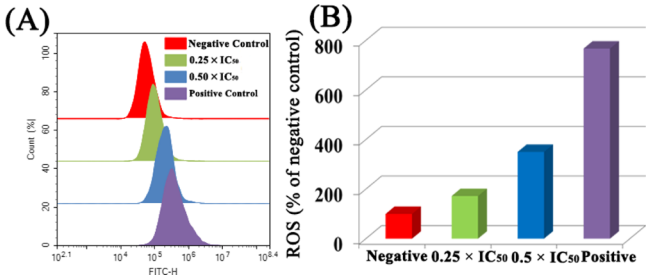

Figure 9. (A) Effect of complex **1** on intracellular ROS levels in A549 lung cancer cells treated at the indicated concentrations for 24 h. (B) Histogram shows the level of ROS induction in A549 cancer cells treated with complex **1**. Data were quoted as the mean ± SD of three replicates.

that the complex can induce an increase in intracellular ROS content, which may be caused by mitochondrial stimulation caused by lysosomal damage, thereby inducing apoptosis.[60] However, there was no significant change in ROS in cells exposed to N̂N ligand complexes A and B. This is an exciting finding that our newly designed synthetic complexes have new advantages in anticancer research. In addition, intracellular ROS, which acts as a second messenger, regulate many key signaling pathways, such as NF-κB. NF-κB is a mammalian transcription factor that controls the expression of cell survival genes and the induction of proinflammatory enzymes and cytokines. Flow cytometry analysis showed that complex **1** significantly increased ROS levels. Excessive ROS can activate the NF-κB channel. Therefore, we used flow cytometry to detect the amount of NF-κBp65 protein in the cells exposed to the complex. Compared with the control group, the content of NF-κBp65 protein in the cells with complexes was significantly increased. However, when *N*-acetylcysteine (a known antioxidant) was added to the cells with complexes, the content of NF-κBp65 protein was not significantly changed compared with the control group (Figure S7). The experimental results indicate that NF-κB activity is increased by ROS regulation, and role of ROS-NF-κB signaling pathway further induces apoptosis.

2.10. Reaction with NADH Studies. Nicotinamide adenine dinucleotide (NADH) is a reduced form of NADH. As NADH and NAD^+ play a crucial role in biocatalysis, an increase in NADH levels indicates the occurrence of metabolic imbalance.[61] Previously, we have reported that NADH can provide hydride to the half-sandwich Ir(III) complex and could produce ROS and H_2O_2. Therefore, monitoring the redox state of NADH is one of the important parameters that characterize the production of ROS.[59] We investigated the reaction of complexes **1** and **2** (1 μM) with NADH (100 μM) in 20% MeOH/80% H_2O (v/v) by UV−Vis at 298 K for 8 h. As the complex reacts with NADH, the turnover number (TONs) of revolutions of complex **1** and complex **2** are calculated using a UV spectrophotometer by calculating the difference in UV absorption at 339 nm (UV absorption peak of NADH) (Figure S8). The TONs of complex **1** (6.10%) and complex **2** (3.21%) were calculated. It is indicated that there is no obvious complex reaction with NADH in this system, which is not the main cause of the increase of intracellular ROS.

2.11. Antimetastatic Properties. Tumor metastasis is an important manifestation of malignant tumors. If tumor cells are repeatedly transferred, the consequences are quite serious. This is a major cause of refractory tumors. Therefore, it is very important to study the mechanism of antitumor drugs against tumor metastasis, so as to screen and develop new drugs that can promote the body's antitumor metastasis.[45] Therefore, we examined the effect of complex **1** on A549 cells using a wound healing assay. During wound healing, the wound healing of A549 cancer cells showed significant antimigration ability after 24 h of treatment compared with the untreated control group (Figure 10). MMPs are a large family that can degrade various

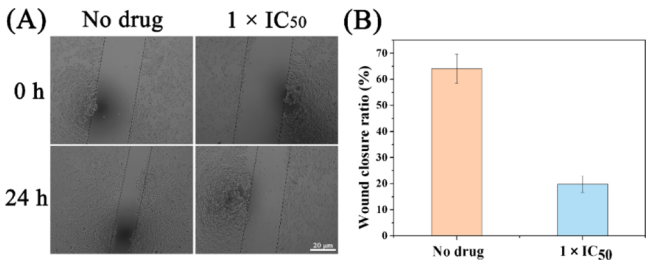

Figure 10. Wound healing assay of A549 cells treated with or without complex **1** for 24 h. (A) Typical images were taken at 0 and 24 h. The widths of wounds are indicated with the lines (μm). Scale bar: 20 μm. (B) Quantification of microscope images. Data are quoted as mean ± SD of three replicates.

protein components in the extracellular matrix, destroy the histological barrier of tumor cell invasion, and play a key role in tumor invasion and metastasis. Among the many MMPs, MMP-9 (matrix metalloproteinase 9) is involved in angiogenesis, directly related to the degradation of the basement membrane, and closely related to tumor metastasis and prognosis.[62−66] In order to further prove that the complex has the antimetastatic ability of cancer cells, we used flow cytometry to detect the content of MMP-9 in the cells exposed to the complex (Figure S9). The experimental results showed

DOI: 10.1021/acsomega.9b01863
ACS Omega 2019, 4, 15240−15248

that intracellular MMP-9 was compared with the blank control group. The content is significantly reduced, thereby inhibiting the migration of cancer cells.

3. CONCLUSIONS

Two kinds of rhodamine-modified half-sandwich (III) complexes with ĈN coordination were designed and synthesized. These complexes have good antiproliferative ability while having good stability and fluorescent properties. Both complexes could be combined with BSA. Subsequently, we also performed a series of bioactivity tests on complex **1** using a cell flow cytometer. Cell cycle, apoptosis, MMP, and ROS were examined. This complex **1** could block the S phase of the cell cycle, promote early and late atrophy, and a significant increase in intracellular ROS, but the interaction with NADH is not obvious, which is also an interesting phenomenon. The experimental results indicate that NF-κB activity is increased by ROS regulation, and the role of ROS-NF-κB signaling pathway further induces apoptosis. Next, confocal microscopy imaging experiments provide a better way to observe the specific anticancer mechanisms of these complexes. The way this complex enters A549 cells is an energy-dependent pathway and preferentially accumulates in lysosomes rather than mitochondria. Because of the difference in fluorophores, the degree of targeting of the complex to lysosomes is also different. These iridium complexes cause cell autolysis and cell death by destroying the lysosomal membrane. Excitingly, the antimigration experiments prove that the iridium complex **1** we designed has good antimigration ability. These rhodamine-modified complexes that target lysosomes may play an important role in the research of anticancer mechanisms and intracellular imaging, and they are promising candidates for future potential anticancer agents for the treatment of cancer.

4. MATERIALS AND METHODS

Detailed synthesis steps for ligands and complexes are provided in the Supporting Information (Figures S10−S14).

L_1: 1.063 g, yield: 89%.^{1}H NMR (500 MHz, $CDCl_3$): δ 8.67 (d, J = 4.6 Hz, 1H), 8.44 (s, 1H), 8.06−8.02 (m, 1H), 7.90 (d, J = 8.3 Hz, 2H), 7.75 (t, J = 7.7 Hz, 1H), 7.69 (d, J = 7.9 Hz, 1H), 7.63 (d, J = 8.3 Hz, 2H), 7.51−7.46 (m, 2H), 7.25−7.22 (m, 1H), 7.07 (dd, J = 5.5, 2.8 Hz, 1H), 6.42 (s, 2H), 6.35 (s, 2H), 3.22 (q, J = 7.1 Hz, 4H), 1.87 (s, 6H), 1.31 (t, J = 7.1 Hz, 6H). Anal. Calcd for L_1: C, 76.87; H, 5.94; N, 11.80. Found: C, 76.78; H, 5.92; N, 11.76.

L_2: 0.852 g, yield: 69%.^{1}H NMR (500 MHz, $CDCl_3$): δ 8.74−8.59 (m, 2H), 8.00 (d, J = 7.7 Hz, 1H), 7.91 (d, J = 8.4 Hz, 2H), 7.74−7.64 (m, 4H), 7.52−7.46 (m, 2H), 7.20 (ddd, J = 6.5, 4.8, 1.4 Hz, 1H), 7.14 (d, J = 6.9 Hz, 1H), 6.57−6.42 (m, 4H), 6.25 (d, J = 8.0 Hz, 2H), 3.32 (q, J = 7.0 Hz, 8H), 1.15 (t, J = 7.0 Hz, 12H). Anal. Calcd for L_2: C, 77.27; H, 6.32; N, 11.26. Found: C, 77.31; H, 6.25; N, 11.20.

$[(\eta^5\text{-}C_5Me_4C_6H_4C_6H_5)Ir(L_1)Cl]PF_6$ (**1**): 0.110 g, yield: 60.25%. ^{1}H NMR (500 MHz, DMSO): δ 8.72 (s, 1H), 8.49 (d, J = 5.7 Hz, 1H), 8.13 (d, J = 8.2 Hz, 1H), 7.91 (d, J = 6.5 Hz, 1H), 7.87−7.81 (m, 2H), 7.74 (d, J = 7.4 Hz, 2H), 7.68−7.56 (m, 6H), 7.48 (t, J = 7.7 Hz, 2H), 7.39 (d, J = 7.3 Hz, 1H), 7.32 (d, J = 8.3 Hz, 2H), 7.19 (t, J = 7.7 Hz, 2H), 7.05 (d, J = 7.0 Hz, 1H), 6.23 (s, 1H), 6.20 (s, 1H), 6.17 (s, 1H), 6.11 (s, 1H), 3.14−3.05 (m, 4H), 1.82 (d, J = 19.8 Hz, 6H), 1.73−1.62 (m, 9H), 1.47 (s, 3H), 1.22−1.14 (m, 6H). Anal. Calcd for $[(\eta^5\text{-}C_5Me_4C_6H_4C_6H_5)Ir(L_1)Cl]$ (1093.37): C, 64.79; H, 5.07; N, 6.40. Found: C, 64.66; H, 5.01; N, 6.20. MS m/z: 1058.92 $[(\eta^5\text{-}C_5Me_4C_6H_4C_6H_5)Ir(L_1)]^+$.

$[(\eta^5\text{-}C_5Me_4C_6H_4C_6H_5)Ir(L_2)Cl]PF_6$ (**2**): 0.080 g, yield: 71.71%. ^{1}H NMR (500 MHz, DMSO): δ 8.94 (s, 1H), 8.46 (d, J = 5.4 Hz, 1H), 8.13 (d, J = 8.1 Hz, 1H), 7.91 (d, J = 7.7 Hz, 1H), 7.84 (dd, J = 18.9, 7.7 Hz, 2H), 7.73 (d, J = 9.5 Hz, 3H), 7.61 (ddd, J = 18.8, 17.3, 8.4 Hz, 5H), 7.48 (t, J = 7.7 Hz, 2H), 7.38 (s, 1H), 7.32 (d, J = 8.3 Hz, 2H), 7.19 (dd, J = 8.3, 4.7 Hz, 2H), 7.11 (d, J = 5.8 Hz, 1H), 6.42 (d, J = 9.0 Hz, 1H), 6.38 (d, J = 8.8 Hz, 1H), 6.36−6.30 (m, 4H), 3.31−3.22 (m, 8H), 1.70 (d, J = 12.5 Hz, 6H), 1.61 (s, 3H), 1.46 (s, 3H), 1.05 (dt, J = 29.8, 7.0 Hz, 12H). Anal. Calcd for $[(\eta^5\text{-}C_5Me_4C_6H_4C_6H_5)Ir(L_2)Cl]$ (1121.40): C, 65.31; H, 5.30; N, 6.24. Found: C, 65.36; H, 5.22; N, 6.18. MS m/z: 1086.05 $[(\eta^5\text{-}C_5Me_4C_6H_4C_6H_5)Ir(L_2)]^+$.

■ ASSOCIATED CONTENT

Supporting Information

The Supporting Information is available free of charge on the ACS Publications website at DOI: 10.1021/acsomega.9b01863.

Detailed experimental procedures, experimental pictures, and related references for the following experiments: UV−vis spectroscopy; stability and fluorescence characteristics of complexes (picture of the stability of complex **2**); BSA binding studies (experimental picture of complex **2**) combined with BSA; cell culture; viability assay (MTT assay); cell cycle analysis (experimental data of the cell cycle); induction of apoptosis (experimental data of apoptosis); cellular localization assay (complexes and mitochondria colocalization picture); mitochondrial membrane assay (picture of the effect of complex **1** on MMP); ROS determination (effect of complex **1** on intracellular NF-κBp65 protein content); reaction with NADH (picture of the complexes reacting with NADH); transwell migration assay (effect of complex **1** on intracellular MMP-9 content); AO assay; and materials and syntheses (mass spectrometry and NMR spectroscopy of complexes) (PDF)

■ AUTHOR INFORMATION

Corresponding Author

*E-mail: liuzheqd@163.com.

ORCID

Zhe Liu: 0000-0001-5796-4335

Notes

The authors declare no competing financial interest.

■ ACKNOWLEDGMENTS

The authors thank the National Natural Science Foundation of China (grant no. 21671118) and the Taishan Scholars Program for support.

■ REFERENCES

(1) Rosenberg, B.; Vancamp, L.; Trosko, J. E.; Mansour, V. H. Platinum compounds: a new class of potent antitumour agents. *Nature* **1969**, *222*, 385−386.

(2) Trosko, N. P. Multi-platinum anti-cancer agents. Substitution-inert compounds for tumor selectivity and new targets. *Chem. Soc. Rev.* **2015**, *44*, 8773−8785.

DOI: 10.1021/acsomega.9b01863
ACS Omega 2019, 4, 15240−15248

(3) Johnstone, T. C.; Suntharalingam, K.; Lippard, S. J. The Next Generation of Platinum Drugs: Targeted Pt(II) Agents, Nanoparticle Delivery, and Pt(IV) Prodrugs. *Chem. Rev.* **2016**, *116*, 3436−3486.
(4) Wang, X.; Wang, X.; Guo, Z. Functionalization of Platinum Complexes for Biomedical Applications. *Acc. Chem. Res.* **2015**, *48*, 2622−2631.
(5) Cheng, Q.; Liu, Y. Multifunctional platinum-based nanoparticles for biomedical applications. *Wiley Interdiscip. Rev.: Nanomed. Nanobiotechnol.* **2017**, *9*, No. e1410.
(6) Li, G.; Chen, Y.; Wang, J.; Lin, Q.; Zhao, J.; Ji, L.; Chao, H. A dinuclear iridium complex as a visual specific phosphorescent probe for endogenous sulphite and bisulphite in living cells. *Chem. Sci.* **2013**, *4*, 4426−4433.
(7) Gao, R.; Ho, D. G.; Hernandez, B.; Selke, M.; Murphy, D.; Djurovich, P. I.; Thompson, M. E. Bis-cyclometalated Ir(III) complexes as efficient singlet oxygen sensitizers. *J. Am. Chem. Soc.* **2002**, *124*, 14828−14829.
(8) He, L.; Li, Y.; Tan, C.-P.; Ye, R.-R.; Chen, M.-H.; Cao, J.-J.; Ji, L.-N.; Mao, Z.-W. Cyclometalated iridium (III) complexes as lysosome-targeted photodynamic anticancer and real-time tracking agents. *Chem. Sci.* **2015**, *6*, 5409−5418.
(9) Li, C.; Yu, M.; Sun, Y.; Wu, Y.; Huang, C.; Li, F. A nonemissive iridium(III) complex that specifically lights-up the nuclei of living cells. *J. Am. Chem. Soc.* **2011**, *133*, 11231−11239.
(10) Tian, M.; Li, J.; Zhang, S.; Guo, L.; He, X.; Kong, D.; Zhang, H.; Liu, Z. Half-sandwich ruthenium (ii) complexes containing N̂N-chelated imino-pyridyl ligands that are selectively toxic to cancer cells. *Chem. Commun.* **2017**, *53*, 12810−12813.
(11) Li, J.; Tian, M.; Tian, Z.; Zhang, S.; Yan, C.; Shao, C.; Liu, Z. Half-Sandwich Iridium (III) and Ruthenium (II) Complexes Containing P̂P-Chelating Ligands: A New Class of Potent Anticancer Agents with Unusual Redox Features. *Inorg. Chem.* **2018**, *57*, 1705−1716.
(12) Wang, C.; Liu, J.; Tian, Z.; Tian, M.; Tian, L.; Zhao, W.; Liu, Z. Half-sandwich iridium N-heterocyclic carbene anticancer complexes. *Dalton Trans.* **2017**, *46*, 6870−6883.
(13) Guan, R.; Chen, Y.; Zeng, L.; Rees, T. W.; Jin, C.; Huang, J.; Chen, Z.-S.; Ji, L.; Chao, H. Oncosis-inducing cyclometalated iridium (III) complexes. *Chem. Sci.* **2018**, *9*, 5183−5190.
(14) Zhang, P.; Chiu, C. K. C.; Huang, H.; Lam, Y. P. K.; Habtemariam, A.; Malcomson, T.; Paterson, M. J.; Clarkson, G. J.; O'Connor, P. B.; Chao, H. Organoiridium Photosensitizers Induce Specific Oxidative Attack on Proteins within Cancer Cells. *Angew. Chem., Int. Ed.* **2017**, *56*, 14898.
(15) Zhong, H.-J.; Lu, L.; Leung, K.-H.; Wong, C. C. L.; Peng, C.; Yan, S.-C.; Ma, D.-L.; Cai, Z.; David Wang, H.-M.; Leung, C.-H. An iridium (iii)-based irreversible protein−protein interaction inhibitor of BRD4 as a potent anticancer agent. *Chem. Sci.* **2015**, *6*, 5400−5408.
(16) Chen, M.-H.; Wang, F.-X.; Cao, J.-J.; Tan, C.-P.; Ji, L.-N.; Mao, Z.-W. Light-Up Mitophagy in Live Cells with Dual-Functional Theranostic Phosphorescent Iridium (III) Complexes. *ACS Appl. Mater. Interfaces* **2017**, *9*, 13304−13314.
(17) Konkankit, C. C.; Marker, S. C.; Knopf, K. M.; Wilson, J. J. Anticancer activity of complexes of the third row transition metals, rhenium, osmium, and iridium. *Dalton Trans.* **2018**, *47*, 9934−9974.
(18) Liu, C.; Yang, C.; Lu, L.; Wang, W.; Tan, W.; Leung, C. H.; Ma, D. L. Luminescent iridium(iii) complexes as COX-2-specific imaging agents in cancer cells. *Chem. Commun.* **2017**, *53*, 2822−2825.
(19) Vellaisamy, K.; Li, G.; Ko, C.-N.; Zhong, H.-J.; Fatima, S.; Kwan, H.-Y.; Wong, C.-Y.; Kwong, W.-J.; Tan, W.; Leung, C.-H.; Ma, D.-L. Cell imaging of dopamine receptor using agonist labeling iridium (iii) complex. *Chem. Sci.* **2018**, *9*, 1119−1125.
(20) Cao, R.; Jia, J.; Ma, X.; Zhou, M.; Fei, H. Membrane Localized Iridium (III) Complex Induces Endoplasmic Reticulum Stress and Mitochondria-Mediated Apoptosis in Human Cancer Cells. *J. Med. Chem.* **2013**, *56*, 3636−3644.
(21) Li, Y.; Tan, C.-P.; Zhang, W.; He, L.; Ji, L.-N.; Mao, Z.-W. Phosphorescent iridium (III)-bis-N-heterocyclic carbene complexes as mitochondria-targeted theranostic and photodynamic anticancer agents. *Biomaterials* **2015**, *39*, 95−104.
(22) Zimbron, J. M.; Passador, K.; Gatin-Fraudet, B.; Bachelet, C.-M.; Plażuk, D.; Chamoreau, L.-M.; Botuha, C.; Thorimbert, S.; Salmain, M. Synthesis, Photophysical Properties, and Living Cell Imaging of Theranostic Half-Sandwich Iridium−4,4-Difluoro-4-bora-3a,4a-diaza-s-indacene (BODIPY) Dyads. *Organometallics* **2017**, *36*, 3435−3442.
(23) Li, J.; Guo, L.; Tian, Z.; Tian, M.; Zhang, S.; Xu, K.; Qian, Y.; Liu, Z. Novel half-sandwich iridium (iii) imino-pyridyl complexes showing remarkable in vitro anticancer activity. *Dalton Trans.* **2017**, *46*, 15520−15534.
(24) Fakih, S.; Podinovskaia, M.; Kong, X.; Collins, H. L.; Schaible, U. E.; Hider, R. C. Targeting the Lysosome: Fluorescent Iron (III) Chelators To Selectively Monitor Endosomal/Lysosomal Labile Iron Pools. *J. Med. Chem.* **2008**, *51*, 4539−4552.
(25) Falgueyret, J.-P.; Desmarais, S.; Oballa, R.; Black, W. C.; Cromlish, W.; Khougaz, K.; Lamontagne, S.; Massé, F.; Riendeau, D.; Toulmond, S.; Percival, M. D. Lysosomotropism of Basic Cathepsin K Inhibitors Contributes to Increased Cellular Potencies against Off-Target Cathepsins and Reduced Functional Selectivity. *J. Med. Chem.* **2005**, *48*, 7535−7543.
(26) Gigli, R.; Pereira, G. J. S.; Antunes, F.; Bechara, A.; Garcia, D. M.; Spindola, D. G.; Jasiulionis, M. G.; Caires, A. C. F.; Smaili, S. S.; Bincoletto, C. The biphosphinic paladacycle complex induces melanoma cell death through lysosomal−mitochondrial axis modulation and impaired autophagy. *Eur. J. Med. Chem.* **2016**, *107*, 245−254.
(27) Chen, Z.; Liang, X.; Zhang, H.; Xie, H.; Liu, J.; Xu, Y.; Zhu, W.; Wang, Y.; Wang, X.; Tan, S.; Kuang, D.; Qian, X. New Class of Naphthalimide-Based Antitumor Agents That Inhibit Topoisomerase II and Induce Lysosomal Membrane Permeabilization and Apoptosis. *J. Med. Chem.* **2010**, *53*, 2589−2600.
(28) Yu, Q.; Liu, Y.; Xu, L.; Zheng, C.; Le, F.; Qin, X.; Liu, Y.; Liu, J. Ruthenium (II) polypyridyl complexes: Cellular uptake, cell image and apoptosis of HeLa cancer cells induced by double targets. *Eur. J. Med. Chem.* **2014**, *82*, 82−95.
(29) Ruiz-González, R.; Acedo, P.; Sánchez-García, D.; Nonell, S.; Cañete, M. C.; Stockert, J. C.; Villanueva, A. Efficient induction of apoptosis in HeLa cells by a novel cationic porphycene photosensitizer. *Eur. J. Med. Chem.* **2013**, *63*, 401−414.
(30) Bechara, A.; Barbosa, C. M. V.; Paredes-Gamero, E. J.; Garcia, D. M.; Silva, L. S.; Matsuo, A. L.; Nascimento, F. D.; Rodrigues, E. G.; Caires, A. C. F.; Smaili, S. S.; Bincoletto, C. Palladacycle (BPC) antitumour activity against resistant and metastatic cell lines: the relationship with cytosolic calcium mobilisation and cathepsin B activity. *Eur. J. Med. Chem.* **2014**, *79*, 24−33.
(31) Marino, J.; García Vior, M. C.; Dicelio, L. E.; Roguin, L. P.; Awruch, J. Photodynamic effects of isosteric water-soluble phthalocyanines on human nasopharynx KB carcinoma cells. *Eur. J. Med. Chem.* **2010**, *45*, 4129−4139.
(32) Ramette, R. W.; Sandell, E. B. Rhodamine B Equilibria. *J. Am. Chem. Soc.* **1956**, *78*, 4872−4878.
(33) Dujols, V.; Ford, F.; Czarnik, A. W. A Long-Wavelength Fluorescent Chemodosimeter Selective for Cu(II) Ion in Water. *J. Am. Chem. Soc.* **1997**, *119*, 7386−7387.
(34) Beija, M.; Afonso, C. A. M.; Martinho, J. M. G. Synthesis and applications of Rhodamine derivatives as fluorescent probes. *Chem. Soc. Rev.* **2009**, *38*, 2410−2433.
(35) Goddard, J.-P.; Reymond, J.-L. Recent advances in enzyme assays. *Trends Biotechnol.* **2004**, *22*, 363−370.
(36) Duong, T. Q.; Kim, J. S. Fluoro- and chromogenic chemodosimeters for heavy metal ion detection in solution and biospecimens. *Chem. Rev.* **2010**, *110*, 6280−6301.
(37) Kwon, J. Y.; Jang, Y. J.; Lee, Y. J.; Kim, K. M.; Seo, M. S.; Nam, W.; Yoon, J. A Highly Selective Fluorescent Chemosensor for Pb2+. *J. Am. Chem. Soc.* **2005**, *127*, 10107−10111.
(38) Wang, C.; Wong, K. M.-C. Bichromophoric rhodamine-iridium (III) sensory system: modulation of the energy-transfer process

DOI: 10.1021/acsomega.9b01863
ACS Omega 2019, 4, 15240−15248

through a selective sensing behavior. *Inorg. Chem.* **2011**, *50*, 5333−5335.
(39) Ma, W.; Tian, Z.; Zhang, S.; He, X.; Li, J.; Xia, X.; Chen, X.; Liu, Z. Lysosome Targeted Drugs: Rhodamine B modified NN-chelating Ligands for Half-sandwich Iridium(III) Anticancer Complexes. *Inorg. Chem. Front.* **2018**, *5*, 2587−2597.
(40) Ma, W.; Ge, X.; Guo, L.; Zhang, S.; Li, J.; He, X.; Liu, Z. Bichromophoric anticancer drug: Targeting lysosome with rhodamine modified cyclometalated Iridium (III) complexes. *Dyes Pigm.* **2019**, *162*, 385−393.
(41) Ma, W.; Guo, L.; Tian, Z.; Zhang, S.; He, X.; Li, J.; Yang, Y.; Liu, Z. Rhodamine-modified fluorescent half-sandwich iridium and ruthenium complexes: potential application as bioimaging and anticancer agents. *Dalton Trans.* **2019**, *48*, 4788−4793.
(42) Novohradsky, V.; Liu, Z.; Vojtiskova, M.; Sadler, P. J.; Brabec, V.; Kasparkova, J. Mechanism of cellular accumulation of an iridium (iii) pentamethylcyclopentadienyl anticancer complex containing a C,N-chelating ligand. *Metallomics* **2014**, *6*, 682−690.
(43) Liu, Z.; Sadler, P. J. Organoiridium Complexes: Anticancer Agents and Catalysts. *Acc. Chem. Res.* **2014**, *47*, 1174−1185.
(44) Liu, Z.; Romero-Canelón, I.; Qamar, B.; Hearn, J. M.; Habtemariam, A.; Barry, N. P. E.; Pizarro, A. M.; Clarkson, G. J.; Sadler, P. J. The potent oxidant anticancer activity of organoiridium catalysts. *Angew. Chem., Int. Ed.* **2014**, *53*, 3941−3946.
(45) Xu, Z.; Kong, D.; He, X.; Guo, L.; Ge, X.; Liu, X.; Zhang, H.; Li, J.; Yang, Y.; Liu, Z. Mitochondria-targeted half-sandwich rutheniumII diimine complexes: anticancer and antimetastasis via ROS-mediated signalling. *Inorg. Chem. Front.* **2018**, *5*, 2100−2105.
(46) Liu, Z.; Sadler, P. J. Organoiridium complexes: anticancer agents and catalysts. *Acc. Chem. Res.* **2014**, *47*, 1174−1185.
(47) Esteghamat-Panah, R.; Hadadzadeh, H.; Farrokhpour, H.; Mortazavi, M.; Amirghofran, Z. A mononuclear Ru(II) complex with meloxicam: DNA- and BSA-binding, molecular modeling and anticancer activity against human carcinoma cell lines. *Inorg. Chim. Acta* **2017**, *454*, 184−196.
(48) Paul, B. K.; Guchhait, N. A spectral deciphering of the binding interaction of an intramolecular charge transfer fluorescence probe with a cationic protein: thermodynamic analysis of the binding phenomenon combined with blind docking study. *Photochem. Photobiol. Sci.* **2011**, *10*, 980−991.
(49) Paul, K. B.; Bhattacharjee, K.; Bose, N.; Guchhait, S. A spectroscopic investigation on the interaction of a magnetic ferrofluid with a model plasma protein: effect on the conformation and activity of the protein. *Phys. Chem. Chem. Phys.* **2012**, *14*, 15482−15493.
(50) Samari, F.; Hemmateenejad, B.; Shamsipur, M.; Rashidi, M.; Samouei, H. Affinity of Two Novel Five-Coordinated Anticancer Pt(II) Complexes to Human and Bovine Serum Albumins: A Spectroscopic Approach. *Inorg. Chem.* **2012**, *51*, 3454−3464.
(51) Shahabadi, N.; Kashanian, S.; Darabi, F. DNA binding and DNA cleavage studies of a water soluble cobalt (II) complex containing dinitrogen Schiff base ligand: the effect of metal on the mode of binding. *Eur. J. Med. Chem.* **2010**, *45*, 4239−4245.
(52) Tabassum, S.; Singh, R.; Zaki, M.; Ahmad, M.; Afzal, M. Synthesis and crystal structure determination of a mononuclear cobalt (II) complex derived from 4-(pyridin-4-ylmethoxy)-benzoic acid: evaluation of the DNA/protein interaction and photo-induced pBR322 DNA cleavage. *RSC Adv.* **2015**, *5*, 35843−35851.
(53) Li, D.; Zhu, M.; Xu, C.; Ji, B. Characterization of the baicalein-bovine serum albumin complex without or with Cu2+ or Fe3+ by spectroscopic approaches. *Eur. J. Med. Chem.* **2011**, *46*, 588−599.
(54) Tang, J.; Luan, F.; Chen, X. Binding analysis of glycyrrhetinic acid to human serum albumin: fluorescence spectroscopy, FTIR, and molecular modeling. *Bioorg. Med. Chem.* **2006**, *14*, 3210−3217.
(55) Yang, Y.; Guo, L.; Tian, Z.; Liu, X.; Gong, Y.; Zheng, H.; Ge, X.; Liu, Z. Imine-N-Heterocyclic Carbenes as Versatile Ligands in Ruthenium (II) p-Cymene Anticancer Complexes: A Structure-Activity Relationship Study. *Chem.—Asian J.* **2018**, *13*, 2923−2933.
(56) Yang, J.; Zhao, J.-X.; Cao, Q.; Hao, L.; Zhou, D.; Gan, Z.; Ji, L.-N.; Mao, Z.-W. Simultaneously Inducing and Tracking Cancer Cell Metabolism Repression by Mitochondria-Immobilized Rhenium (I) Complex. *ACS Appl. Mater. Interfaces* **2017**, *9*, 13900−13912.
(57) Daum, S.; Reshetnikov, V.; Sisa, M.; Dymych, T.; Lootski, M. D.; Bilyy, R.; Bila, E.; Janko, C.; Alexiou, C.; Mortin, H.; Sellner, L.; Mokhir, A. Lysosome-targeting amplifiers of reactive oxygen species as anticancer prodrugs. *Angew. Chem.* **2017**, *129*, 15751−15755.
(58) Jung, K.-Y.; Wang, H.; Teriete, P.; Yap, J. L.; Chen, L.; Lanning, M. E.; Hu, A.; Lambert, L. J.; Holien, T.; Sundan, A.; Cosford, N. D. P.; Prochownik, E. V.; Fletcher, S. Perturbation of the c-Myc-Max protein-protein interaction via synthetic α-helix mimetics. *J. Med. Chem.* **2015**, *58*, 3002−3024.
(59) Liu, Z.; Romero-Canelón, I.; Qamar, B.; Hearn, J. M.; Habtemariam, A.; Barry, N. P. E.; Pizarro, A. M.; Clarkson, G. J.; Sadler, P. J. The potent oxidant anticancer activity of organoiridium catalysts. *Angew. Chem., Int. Ed.* **2014**, *53*, 3941−3946.
(60) Yuan, X.-M.; Li, W.; Dalen, H.; Lotem, J.; Kama, R.; Sachs, L.; Brunk, U. T. Lysosomal destabilization in p53-induced apoptosis. *Proc. Natl. Acad. Sci. U.S.A.* **2002**, *99*, 6286−6291.
(61) Zhang, Y.; Zhang, S.; Tian, Z.; Li, J.; Xu, Z.; Li, S.; Liu, Z. Phenoxide chelated Ir(iii) N-heterocyclic carbene complexes: synthesis, characterization, and evaluation of their in vitro anticancer activity. *Dalton Trans.* **2018**, *47*, 13781−13787.
(62) Wu, K.-J.; Zhong, H.-J.; Yang, G.; Wu, C.; Huang, J.-M.; Li, G.; Ma, D.-L.; Leung, C.-H. Small Molecule Pin1 Inhibitor Blocking NF-κB Signaling in Prostate Cancer cells. *Chem.—Asian J.* **2018**, *13*, 275−279.
(63) Hsu, C.-C.; Lien, J.-C.; Chang, C.-W.; Chang, C.-H.; Kuo, S.-C.; Huang, T.-F. Yuwen02f1 suppresses LPS-induced endotoxemia and adjuvant-induced arthritis primarily through blockade of ROS formation, NFkB and MAPK activation. *Biochem. Pharmacol.* **2013**, *85*, 385−395.
(64) Wu, K.-J.; Zhong, H.-J.; Li, G.; Liu, C.; Wang, H.-M. D.; Ma, D.-L.; Leung, C.-H. Structure-based identification of a NEDD8-activating enzyme inhibitor via drug repurposing. *Eur. J. Med. Chem.* **2018**, *143*, 1021−1027.
(65) Huang, Q.; Zhan, L.; Cao, H.; Li, J.; Lyu, Y.; Guo, X.; Zhang, J.; Ji, L.; Ren, T.; An, J.; Liu, B.; Nie, Y.; Xing, J. Increased mitochondrial fission promotes autophagy and hepatocellular carcinoma cell survival through the ROS-modulated coordinated regulation of the NFKB and TP53 pathways. *Autophagy* **2016**, *12*, 999−1014.
(66) Nishanth, R. P.; Jyotsna, R. G.; Schlager, J. J.; Hussain, S. M.; Reddanna, P. Inflammatory responses of RAW 264.7 macrophages upon exposure to nanoparticles: Role of ROS-NFκB signaling pathway. *Nanotoxicology* **2011**, *5*, 502−516.

DOI: 10.1021/acsomega.9b01863
ACS Omega 2019, 4, 15240−15248